Electronic Supplementary Information

Exploring solvent dependent catecholase activity in transition metal complexes: An experimental and theoretical approach

Mantasha I.[a], M. Shahid[a†], Azaj Ansari[b], Manjeet Kumar[b], Muhammad Nadeem Akhtar[c], Murad A. AlDamen[d], You Song[e], Musheer Ahmad[f], Ishaat M. Khan[a]

[a]Department of Chemistry, Aligarh Muslim University, Aligarh-202002, India

[b]Department of Chemistry, Central University of Haryana, Mahendergarh-123031, Haryana, India

[c]Department of Chemistry, Khwaja Fareed University of Engineering & Information Technology, Rahim Yar Khan 64200, Pakistan.

[d]Department of Chemistry, Faculty of Science, the University of Jordan, Amman 11942, Jordan

[e]State Key Laboratory of Coordination Chemistry, Nanjing University Xianlin Road No. 163, Qixia District, Nanjing 210023 P. R. China

[f]Department of Applied Chemistry (ZHCET), Aligarh Muslim University, Aligarh-202002, India

†Corresponding author, E-mail: shahid81chem@gmail.com

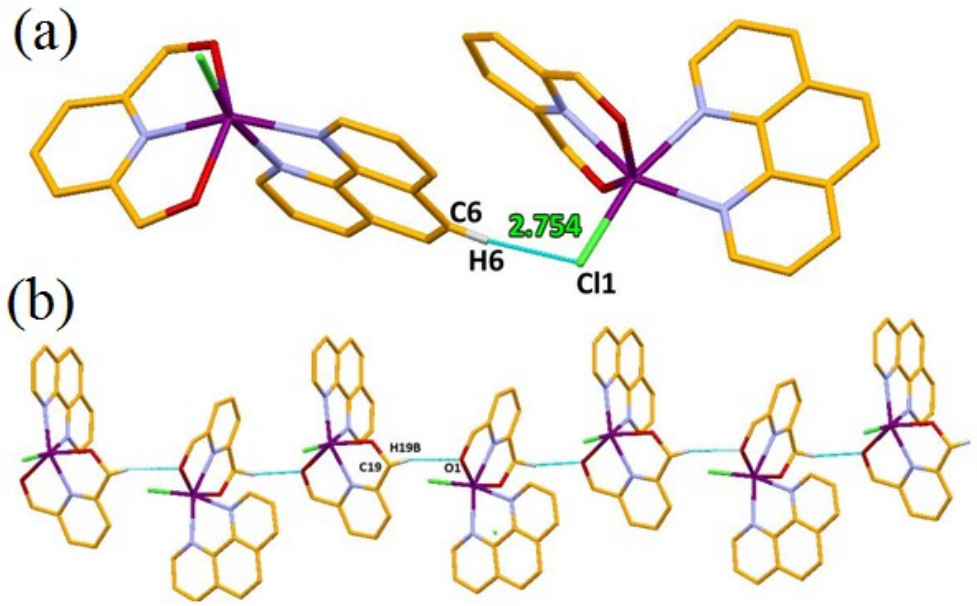

Fig. S1. (a) 1D chain formed through C–H···Cl interaction (b) 1D chain formed through C–H···O interaction in **1**.

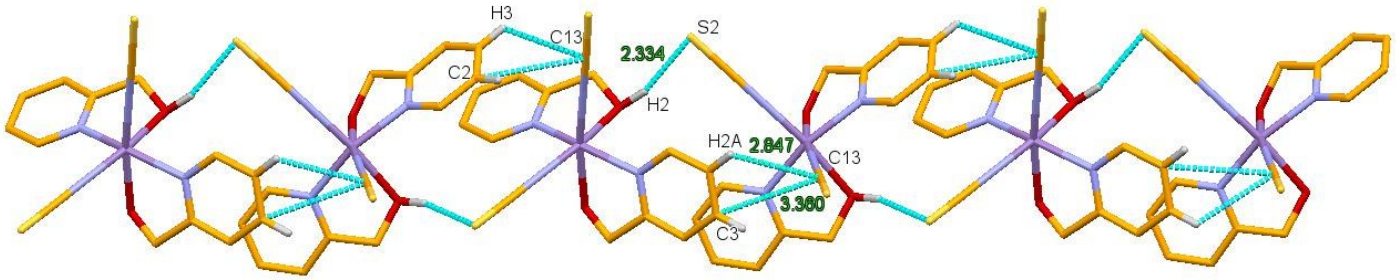

Fig. S2. 1D chain formed O–H···S, C–H···C and H–C···π interactions in **2**.

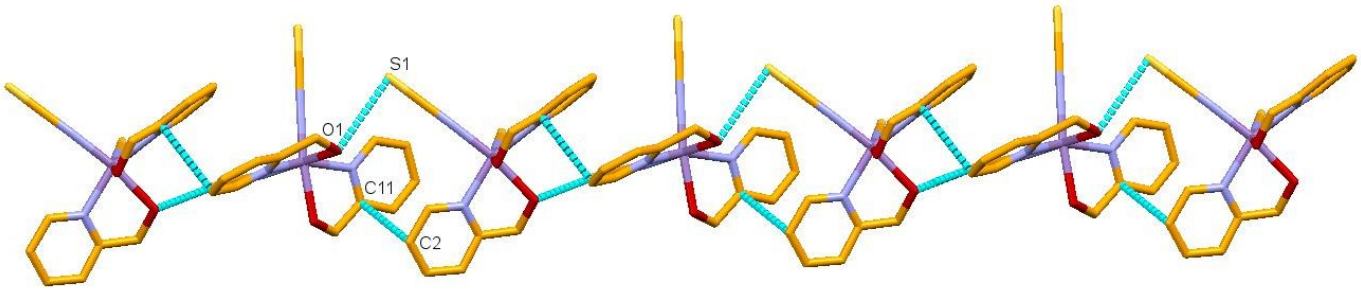

Fig. S3. 1D polymeric chain formed through π-π stacking and O1···S1 interactions in **2**.

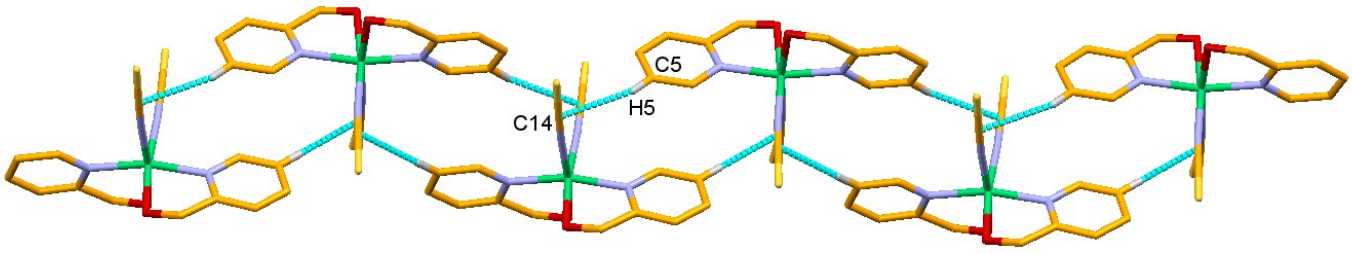

Fig. S4.Formation of 1D chain through C–H···C interaction in **3**.

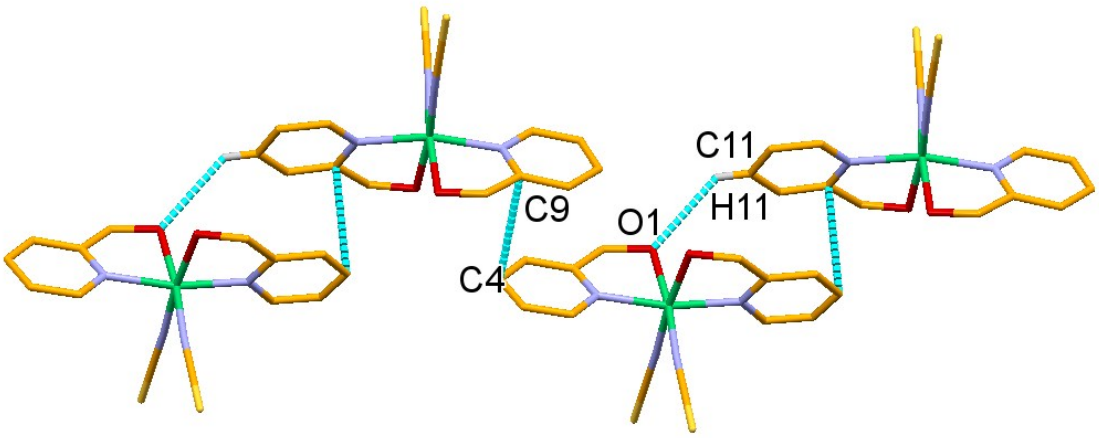

Fig. S5. Formation of 1D chain through π-π stacking and C11–H11···O1 in **3**.

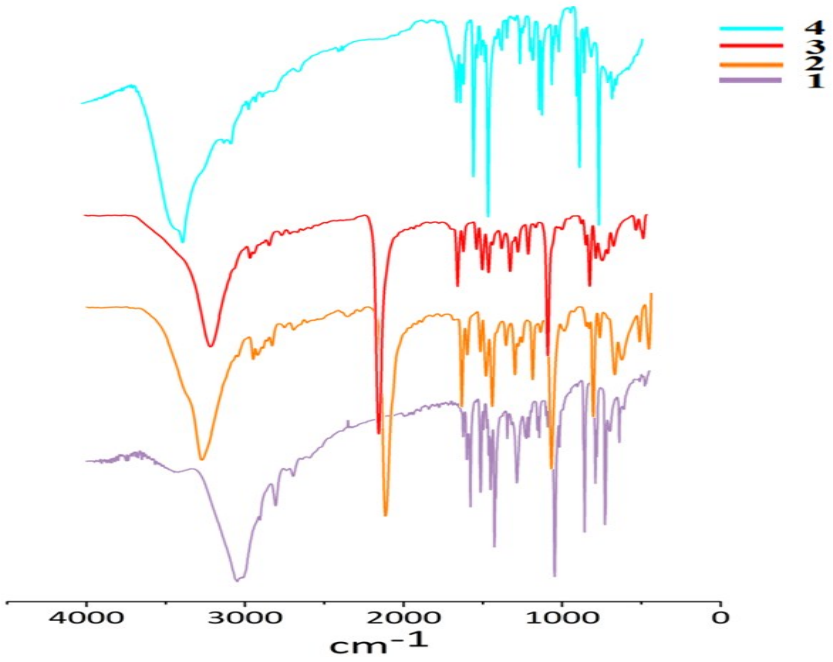

Fig. S6. FTIR spectra of **1**–**4**.

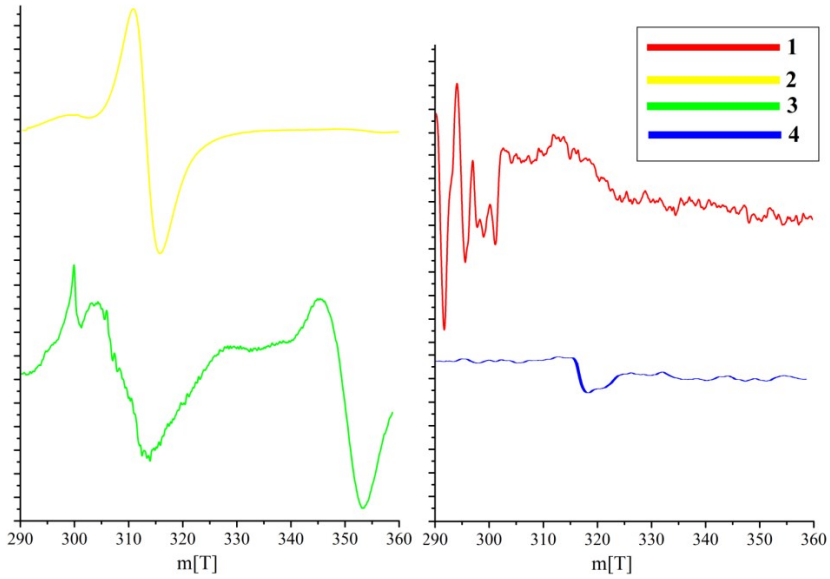

Fig. S7. EPR spectra of **1**–**4**.

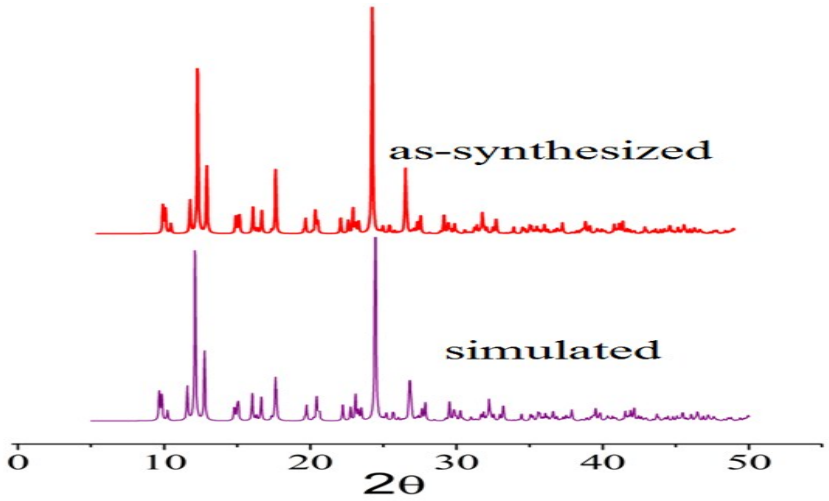

Fig. S8. PXRD pattern of **1**.

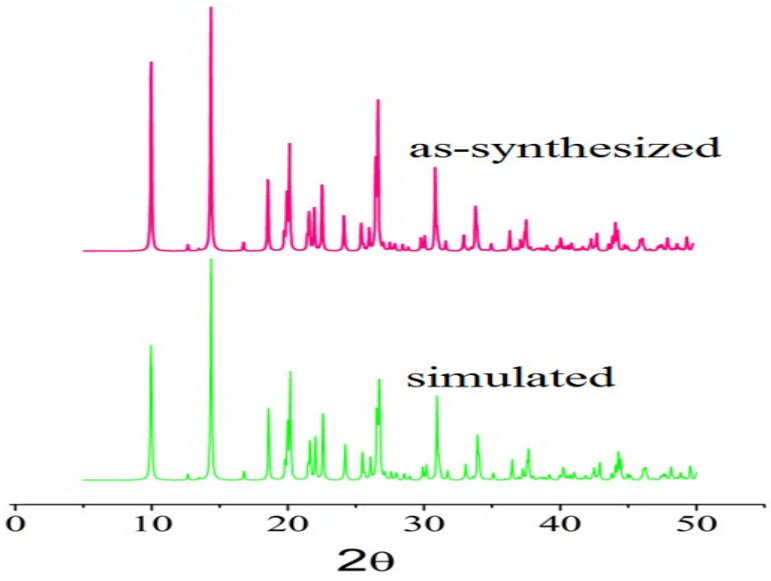

Fig. S9. PXRD pattern of **2**.

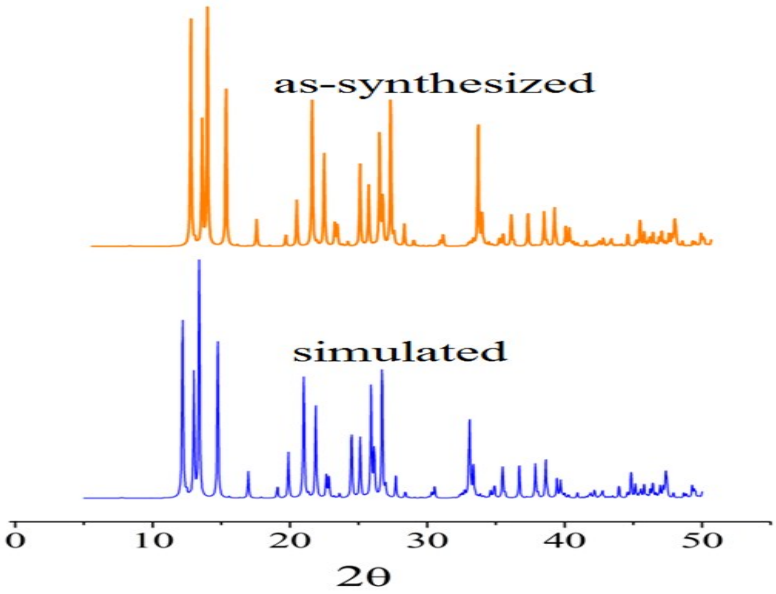

Fig. S10. PXRD pattern of **3**.

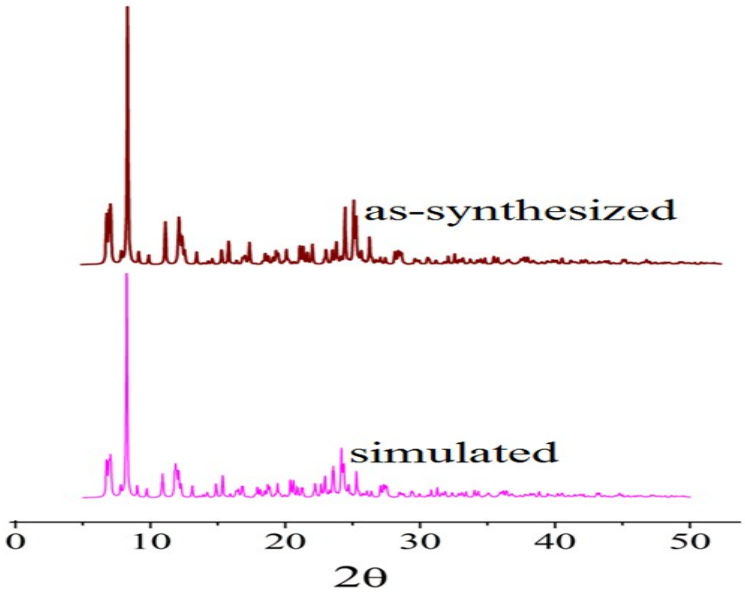

Fig. S11. PXRD pattern of **4**.

TableS1. Selected bond lengths and bond anglesin**1–4.**

Bond Angle(°)									
1		**2**		**3**				**4**	
N1−Mn1−N3	88.48(7)	N4 –Mn1–N3	97.92(12)	N2–Ni1–N2	94.88(11)	N4–Ni2–N4	93.95(11)	N2−Zn1−N1	77.19(12)
N1−Mn1−N2	72.82(7)	N4–Mn1–N2	97.18(12)	N2–Ni1–N1	94.99(7)	N4–Ni2–N3	95.37(7)	N3−Zn1−N1	96.16(11)
N1−Mn1−Cl1	166.45(5)	N3 –Mn1–N2	99.64(12)	N1–Ni1–N1	168.14(10)	N4–Ni2–N3	93.70(7)	N5−Zn1−N1	163.73(12)
N1−Mn1−O1	86.56(7)	N4–Mn1–N1	99.82(12)	N2–Ni1–O1	172.20(7)	N4 –Ni2–N3	93.70(7)	N4−Zn1−N1	94.45(11)
N1−Mn1−O2	90.28(8)	N3–Mn1–N1	96.81(12)	N1–Ni1–O1	93.38(6)	N4 –Ni2–N3	95.37(7)	N6−Zn1−N1	93.10(12)
N2−Mn1−N3	155.82(7)	N2–Mn –N1	154.41(12)	O1–Ni1–O1	88.00(9)	N3–Ni2–N3	166.69(10)	N3−Zn1−N2	91.75(12)
N2−Mn1−Cl1	94.88(5)	N4–Mn–O2	172.18(11)	N2–Ni1–N1	93.03(7)	N4–Ni2–O2	88.94(7)	N4−Zn1−N2	165.76(12)
N2−Mn1−O2	92.87(7)	N3–Mn1–O2	85.10(11)	N2–Ni1–N1	93.03(7)	N4–Ni2–O2	173.12(6)	N5−Zn1−N2	90.56(13)
N2−Mn1−O1	121.04(7)	N2–Mn–O2	75.17(11)	N2–Ni1–N1	94.99(7)	N3–Ni2–O2	92.24(6)	N6−zn1−N2	96.46(12)
O1−Mn1−O2	142.97(7)	N1–Mn1–O2	86.92(11)	N2–Ni1–O1	88.98(7)	N3–Ni2–O2	78.20(6)	N4−Zn1−N3	77.55(12)
N3−Mn1−O2	71.55(7)	N4–Mn1–O1	84.92(11)	N1–Ni1–O1	78.02(6)	N4–Ni2–O2	173.12(6)	N5−Zn1−N3	94.86(13)
N3−Mn1−O1	71.48(7)	N3–Mn1–O1	171.79(11)	N2–Ni1–O1	88.98(7)	N4–Ni2–O2	88.94(7)	N6−Zn1−N3	168.79(12)
N3−Mn1−Cl1	104.86(5)	O2–Mn1–O1	93.08(10)	N2–Ni1–O1	172.20(7)	N3–Ni2–O2	78.20(6)	N5−Zn1−N4	99.60(12
O2−Mn1−Cl1	96.12(7)	N2–Mn1–O1	87.59(11)	N1–Ni1–O1	93.38(6)	N3–Ni2–O2	92.24(6)	N6−Zn1−N4	95.47(11)
O1−Mn1−Cl1	95.34(5)	N1–Mn1–O1	75.08(11)	N1–Ni1–O1	78.02(6)	O2–Ni2–O2	88.89(9) 2	N6−Zn1−N5	77.50(13)

Bond length(Å)							
1		**2**		**3**		**4**	
Mn1−N1	2.2987(19)	Mn1−N1	2.093(3)	Ni1−N1	2.0558(17)	Zn1−N1	2.161(3)
Mn1−N2	2.2443(19)	Mn1−N2	2.091(3)	Ni1−N2	2.034(2)	Zn1−N2	2.184(3)
Mn1−N3	2.2238(19)	Mn1−N3	2.038(3)	Ni2−N3	2.0595(17)	Zn1−N3	2.167(3)
MN1−O1	2.2318(18)	Mn1−N4	2.037(3)	Ni2−N4	2.0220(19)	Zn1−N4	2.151(3)
Mn1−O2	2.1936(19)	Mn1−O1	2.230(3)	Ni1−O1	2.1243(16)	Zn1−N5	2.146(3)
MN1−Cl1	2.4134(8)	Mn1−O2	2.230(3)	Ni2−O2	2.1204(15)	Zn1−N6	2.180(3)

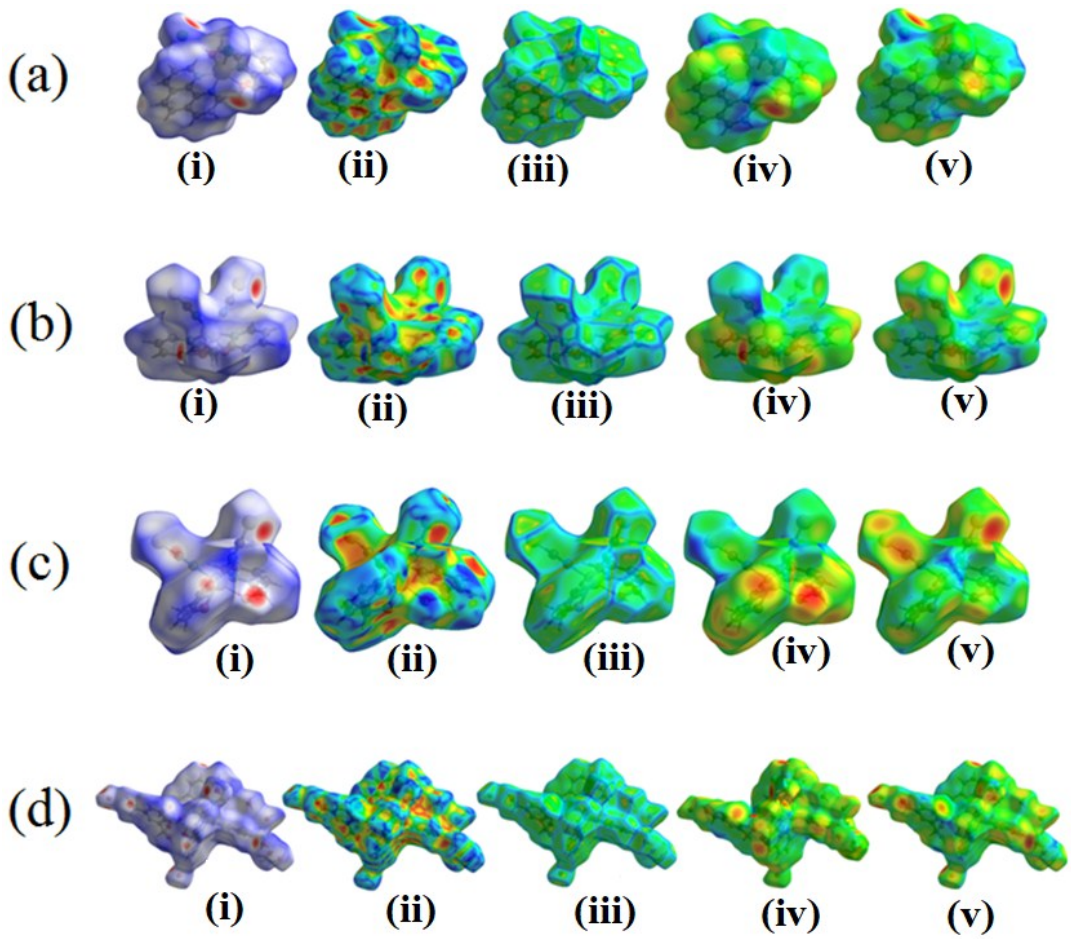

Fig. S12. Molecular Hirshfeld surfaces mapped over (i) d_{norm} (ii) shape index, (iii) curvedness,(iv) $d_i$and (v) $d_e$of (a)**1** (b) **2** (c) **3** (d) **4**.

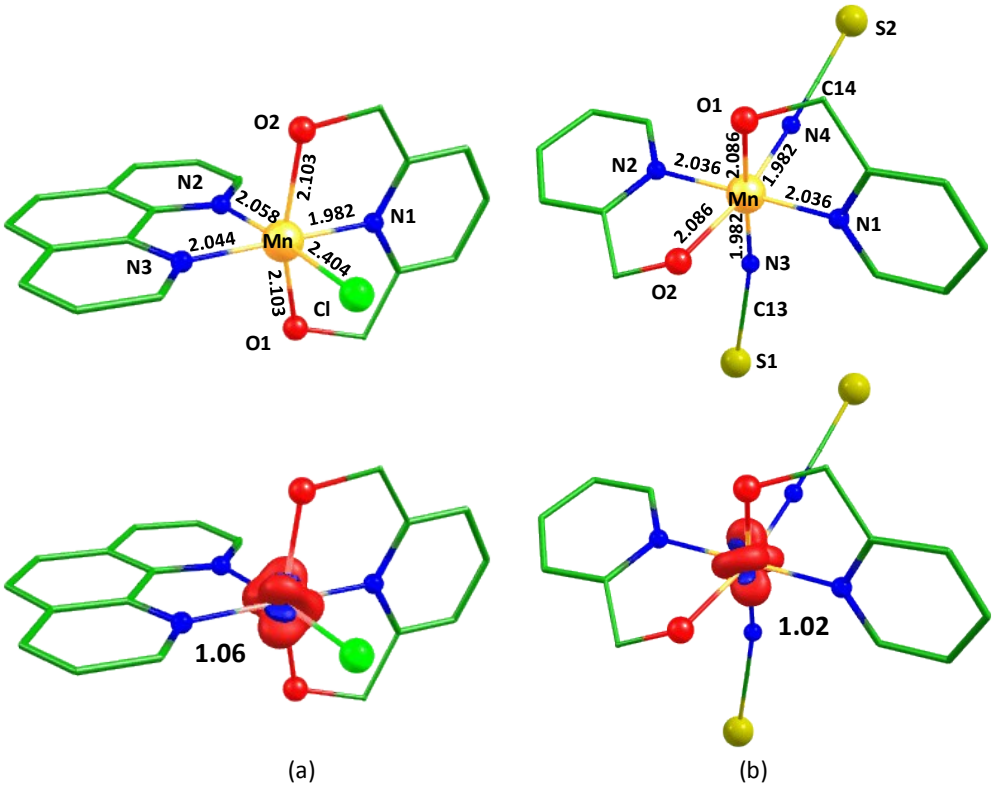

Fig. S13. B3LYP optimized structures and their corresponding spin density plots of the low spin state of (a) **1** and (b) **2**.

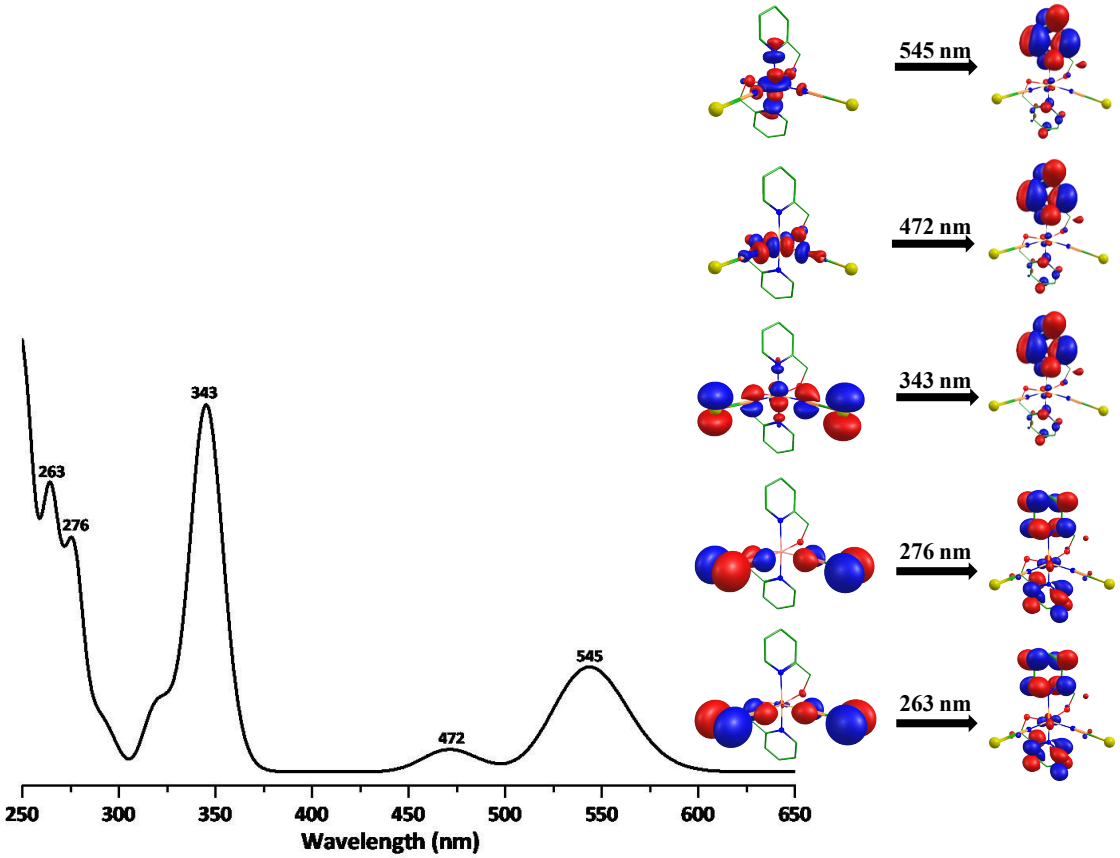

Fig. S14. B3LYP – TD-DFT simulated electronic absorption spectra of high spin state (S=5/2) of **2** and its corresponding orbitals involved in the transitions.

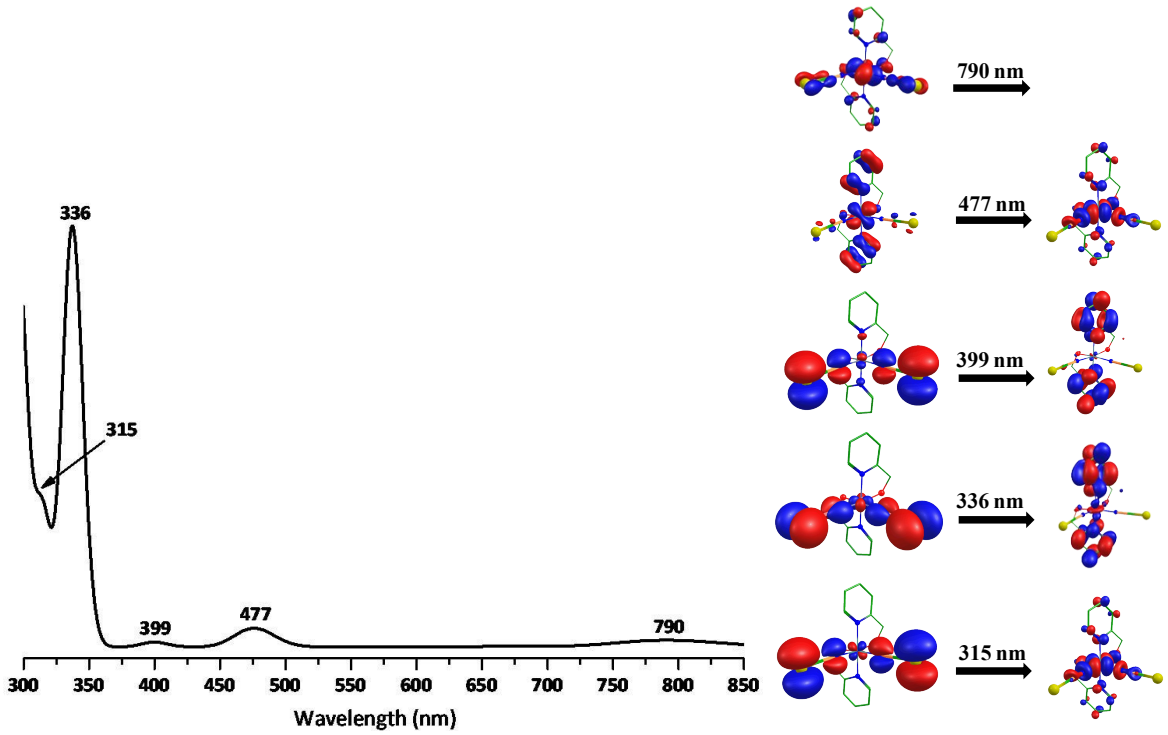

Fig. S15. B3LYP – TD-DFT simulated electronic absorption spectra of high spin state (S=1) of **3** and its corresponding orbitals involved in the transitions.

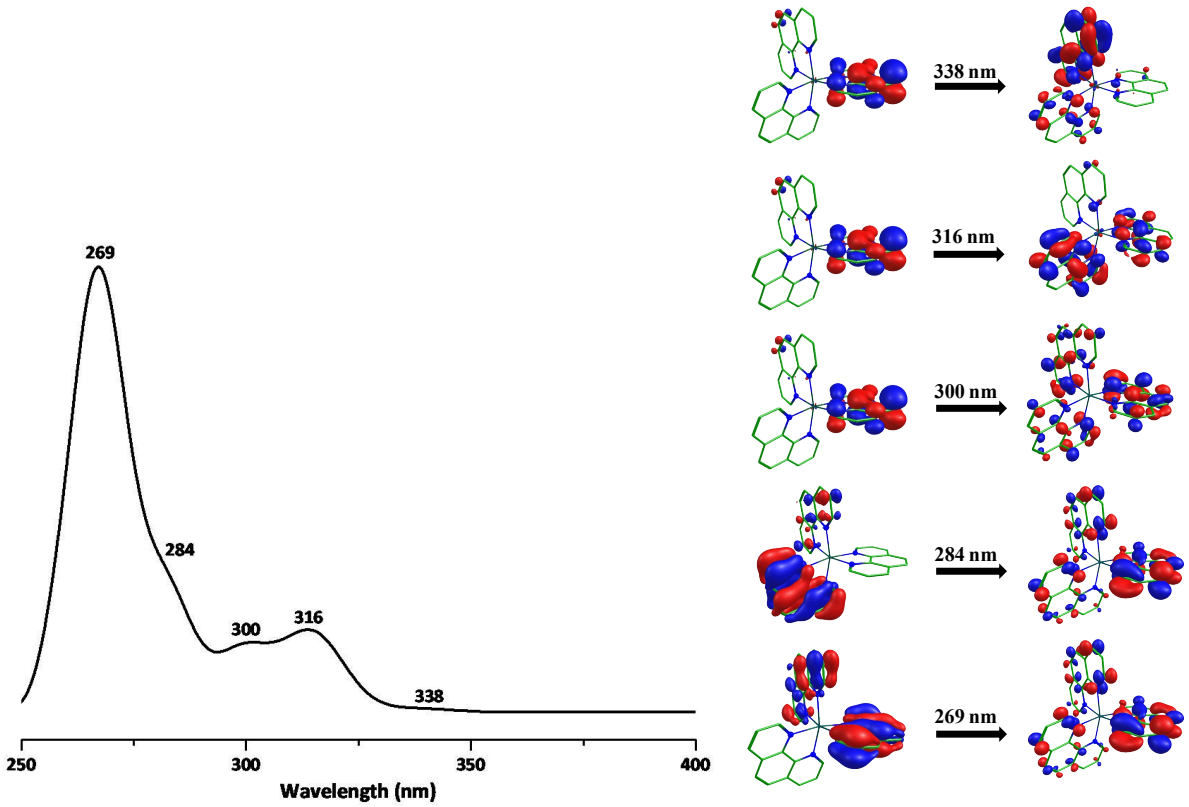

Fig. S16. B3LYP – TD-DFT simulated electronic absorption spectra of **4** and its corresponding orbitals involved in the transitions.